MASSACHUSETTS INSTITUTE OF TECHNOLOGY
ARTIFICIAL INTELLIGENCE LABORATORY

A.I. Memo 771 March, 1984

Basic Solid Mechanics for Tactile Sensing

Ronald S. Fearing

John M. Hollerbach

Abstract. In order to stably grasp objects without using object models, tactile feedback from the fingers is sometimes necessary. This feedback can be used to adjust grasping forces to prevent a part from slipping from a hand. If the angle of force at the object finger contact can be determined, slip can be prevented by the proper adjustment of finger forces. Another important tactile sensing task is finding the edges and corners of an object, since they are usually feasible grasping locations.

This paper describes how this information can be extracted from the finger-object contact using strain sensors beneath a compliant skin. For determining contact forces, strain measurements are easier to use than the surface deformation profile. The finger is modelled as an infinite linear elastic half plane to predict the measured strain for several contact types and forces. The number of sensors required is less than has been proposed for other tactile recognition tasks.

A rough upper bound on sensor density requirements for a specific depth is presented that is based on the frequency response of the elastic medium. The effects of different sensor stiffnesses on sensor performance are discussed.

Acknowledgments. This report describes research done in the Artifical Intelligence Laboratory of the Massachusetts Institute of Technology. Part of the research reported here was carried out while one of the authors (RSF) was a co-op student with General Electric Corporate Research and Development, Schenectady, NY. Support for John Hollerbach was provided by the Systems Development Foundation.

1.0 Introduction

Much of the recent work in tactile sensing has been devoted to recognizing objects and features. One method is to obtain an image-like array of an object profile using high density tactile sensors [Hillis, 1981; Overton and Williamsm 1981]. This is useful for identifying the location, orientation and shape of an object with complicated surfaces, or identifying surface defects. Another approach to the recognition problem uses local low level tactile information and object models to recognize objects [Gaston and Lozano-Perez, 1983].

There are some low level tactile sensing operations that are useful for basic grasping, where the intent is keeping an object stably grasped in a hand, rather than recognizing it. The requirements for grasping polyhedra on a plane with two fingers without object models have been described elsewhere [Fearing, 1984]. The most useful parameters to know are the surface normals, the angle and magnitude of a force at a contact, and whether the finger is touching a corner or edge. These parameters are a subset of those required to recognize general features.

This paper attempts to show how this grasping information can be recovered using a simplified solid mechanics model and basic contact theory. Consideration of the mechanics has been infrequent in the design and use of tactile sensors, (an exception is Kinoshita [1977]), but is important for relating sensory data to physical observables. There has been some work on sensing forces at fingers using tactile sensation to prevent slip [Stojiljkovic and Clot, 1977]. Other techniques have relied on using rollers to detect the slip of an object in parallel jaw grippers [Masuda, Hasegawa, and Osako 1976]. At a more advanced level, the tactile array approach will provide useful information for manipulation, such as finding a specific feature that is crucial to orienting a part accurately.

A finger must have a compliant covering to take advantage of the increased prehension stability possible at corners [Fearing, 1983]. Another advantage of a soft skin is that contact areas are large enough to distinguish between features. For example, with a very hard skin, an edge and a side will contact with the finger at only a few points, and so may be indistinguishable without finger motion. To distinguish between them, it will be necessary to get either the displacement profile or the contact stresses in a compliant finger covering.

There are two different approaches to the tactile transduction problem. The first approach is based on measuring the deflection of a flexible membrane when it contacts a rigid object, or the height of pegs touching an object [Page, Pugh, and Heginbotham, 1976]. The measurement is sometimes done by an optical sensing scheme [Ozaki,Waku and Mohri, 1982]. The second approach is based on forces beneath the surface changing electrical contact areas [Hillis, 1981], or compressing some resistive material without changing the electrical contacts.

We are interested in determining the actual contact stresses rather than just the contact profile. Although the profile aids in recognition of an object shape, it is only indirectly useful for determining the grasping forces. The problem is the indirect relation between the shape of the object and the profile of deformation, especially when there are both normal and tangential forces applied at the contact. Because the compliant material is not perfectly compressible, it will tend to pile up outside the contact region in a complicated manner.

A mathematical problem with treating the contact as a deformation is that superposition does not hold. In general, forces superimpose, but displacements do not. For example, the stresses due to two points close together each indenting 1 mm. into an elastic medium are not equivalent to the sum of the stresses from each point indenting 1 mm. by itself.

Consider a grain of sand pressed between a finger and a smooth surface. A profile change due to the height of the grain is very small, but high stress concentrations near the edges should be readily detectable. One researcher notes that a ridge of less than 20 μm height is perceptible for humans [Lederman, 1978].

2.0 Using Strain for Tactile Sensing

When determining contact stresses, there are practical reasons for measuring these stresses beneath the elastic material, rather than on the surface. Since we may be interested in both normal and tangential (friction) forces at the contact, we would need two different types of sensor at the surface. When sharp rigid objects indent an elastic material, very high stresses are developed at the surface. These stresses are reduced by distance from the application area, so a fragile sensor would be better protected beneath a layer of skin. We note that biological tactile sensors are beneath the surface of the skin. A rather complete analytical and experimental study of stresses beneath the skin and the mechanoreceptor responses to contacts without tangential forces was done by Phillips and Johnson [1981].

The general three dimensional analysis of stress and strain leads to very complicated expressions. If contact forces are constant along a finger, a two dimensional analysis will describe the behavior in a slice perpendicular to the finger axis. In the remainder of this paper we analyze line, edge, and plane contacts for which a 2 dimensional analysis is exact for infinitely long contacts, such as a line load, and approximate for short contact lengths. We will speak of a point indenter or point force while meaning a planar section of a line contact.

We now examine the 2 dimensional behavior of an infinite homogeneous elastic medium for the simplest contact case, a point force with negligible contact area. To find the stresses within the elastic half plane, we first find the stress distribution due to a concentrated normal force at the surface, as in Figure 1. The internal stresses due to a general contact stress on the surface can be found from the superposition principle.

The analysis from Timoshenko [1951] shows that the internal stresses have a "simple radial distribution". That is, all the stress is in the direction of a radial line from the point of application of the force.

From Timoshenko [1951], for the concentrated normal force we get

$$\sigma_r = \frac{-2P}{\pi}\frac{\cos\theta}{r}$$

$$\sigma_\theta = 0$$

$$\tau_{r\theta} = 0 \qquad (1)$$

where σ_r is the radial stress at (r, θ), σ_θ is the stress in the plane at (r, θ) normal to the radial stress, $\tau_{r\theta}$ is the shearing stress in the r,θ plane, P is the force per length, and r is the distance from the point of application.

For a force inclined from the vertical by the angle α,

$$\sigma_r = \frac{-2P}{\pi r}\cos(\alpha+\theta)$$

$$\sigma_\theta = 0 \qquad (2)$$

$$\tau_{r\theta} = 0$$

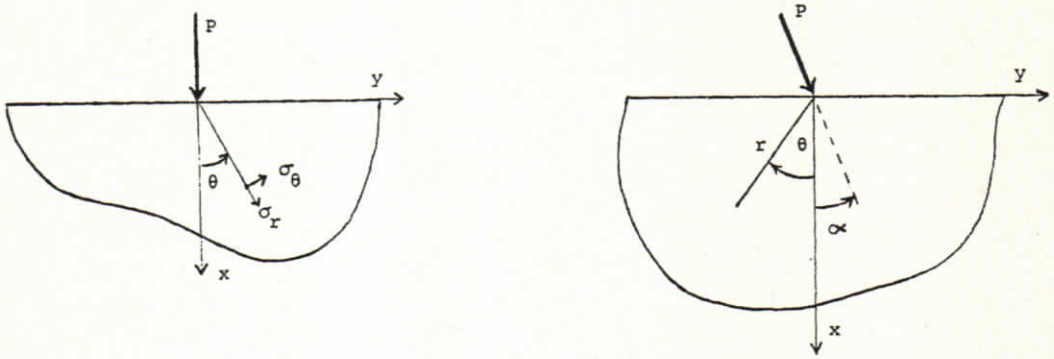

Figure 1. Point Forces on Elastic Half Plane

To get stresses in cartesian coordinates, we apply the tensor transformation:

$$\sigma_x = \sigma_r \cos^2\theta$$

$$\sigma_y = \sigma_r \sin^2\theta$$

$$\tau_{xy} = \sigma_r \sin\theta\cos\theta \qquad (3)$$

So finally, the internal stress due to a point force is:

$$\sigma_x = \frac{-2P}{\pi r} \cos(\alpha+\theta)\cos^2\theta$$

$$\sigma_y = \frac{-2P}{\pi r} \cos(\alpha+\theta)\sin^2\theta$$

$$\tau_{xy} = \frac{-2P}{\pi r} \cos(\alpha+\theta)\sin\theta\cos\theta \qquad (4)$$

where

$$r = \sqrt{x^2 + y^2}$$

$$\cos\theta = \frac{x}{r}, \quad \sin\theta = \frac{y}{r}, \quad \cos(\alpha+\theta) = \frac{x}{r}\cos\alpha - \frac{y}{r}\sin\alpha$$

All pressure sensors have an output based on the strain of the sensor, which is the fractional change in the linear dimensions of a small cubic volume element. This volume change is to first order independent of the shear stresses, which change the angles of the faces in the cube, and not

the dimensions. If we assume a linear elastic medium, we can apply Hooke's Law:

$$\varepsilon_x = \frac{\sigma_x}{E} \tag{5}$$

where E is the modulus of elasticity (N/m^2), and ε_x is the strain along the x axis.

For materials that are not completely compressible, a contraction along one dimension will be coupled with expansions along the other two. For an incompressible cube which undergoes a strain of 1% along one axis, there must be corresponding strains in the opposite sense of about .5% along the other two axes to maintain constant volume. The ratio of these two strains is called Poisson's ratio, and characterizes the compressibility of the material. For a completely compressible material, Poisson's ratio is 0. For a medium that does not change in volume with compression, such as a water filled sack or rubber, Poisson's ratio can be taken as 0.5. Since rubber-like materials are popular for covering robot fingers and tactile sensors this assumption will be used.

The relations between the stresses and strains are (Timoshenko and Goodier 1951):

$$\begin{aligned}
\varepsilon_x &= \frac{1}{E}\left[\sigma_x - \nu(\sigma_y + \sigma_z)\right] \\
\varepsilon_y &= \frac{1}{E}\left[\sigma_y - \nu(\sigma_x + \sigma_z)\right] \\
\varepsilon_z &= \frac{1}{E}\left[\sigma_z - \nu(\sigma_x + \sigma_y)\right]
\end{aligned} \tag{6}$$

where ν is Poisson's ratio=.5, and ε is the strain along one dimension.

There are two simplifying assumptions that can be applied to elasticity problems with the appropriate symmetry. For an infinite line force on an elastic half space, the strain in the direction of the line must be zero by symmetry. This is the plane strain assumption. Alternatively consider a slice of unit width out of the elastic half space, with a line load acting on it. On the faces of this slice, the stresses normal to the face must be zero to satisfy the boundary conditions. This is the plane stress assumption.

For this analysis, we will assume a state of plane strain; there is no strain in the z direction. This assumption will be reasonable if the contacts are long compared to the finger radius. Phillips and Johnson [1981] found that an assumption of plane stress had a better qualitative agreement with the response of mechanoreceptors in finger skin, but the plane strain assumption will be used here because the contacts are assumed to be infinitely long. The form of the strains under these two assumptions is similar.

So from the plane strain assumption $\varepsilon_z = 0$,

$$\sigma_z = \frac{1}{2}(\sigma_x + \sigma_y)$$

$$\begin{aligned}
\varepsilon_x &= \frac{1}{E}\left[\sigma_x - \frac{1}{2}\left[\sigma_y + \frac{\sigma_x + \sigma_y}{2}\right]\right] = \frac{3}{4E}(\sigma_x - \sigma_y) \\
\varepsilon_y &= \frac{1}{E}\left[\sigma_y - \frac{1}{2}\left[\sigma_x + \frac{\sigma_x + \sigma_y}{2}\right]\right] = \frac{3}{4E}(\sigma_y - \sigma_x)
\end{aligned} \tag{7}$$

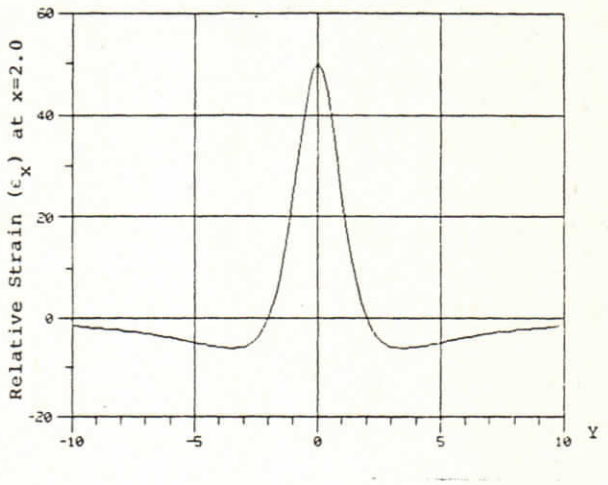

Figure 2. Strain for Line Load Normal to Surface

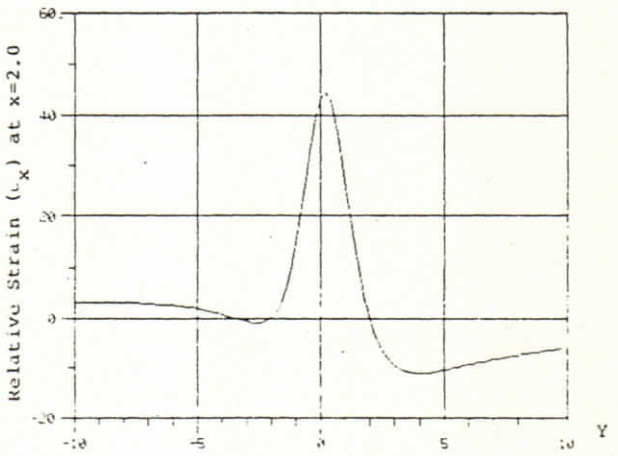

Figure 3. Strain for Line Load Inclined 30 Degrees

For the stresses due to the point indentor or line load (4), the strains from (7) become:

$$\epsilon_x = \frac{3}{4E}\left[\frac{-2P}{\pi r}\cos(\alpha+\theta)\right]\left[\cos^2\theta-\sin^2\theta\right]$$

$$= \frac{-3P}{2\pi Er^4}\left[x\cos\alpha - y\sin\alpha\right]\left[x^2-y^2\right]$$

for $\alpha = 0$

$$\epsilon_x = \frac{-3P}{2\pi Er^4}\, x\,(x^2-y^2) \tag{8}$$

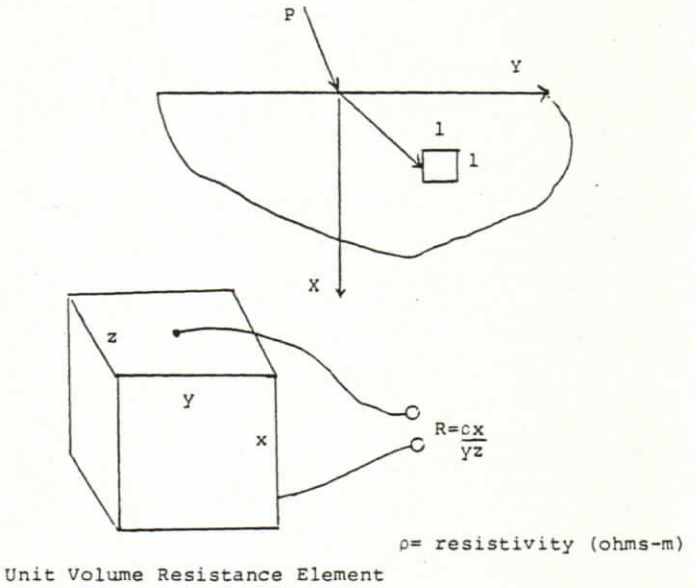

Figure 4. Strain Sensor Based on Resistance

Figures 2 and 3 show the strains in the homogeneous elastic medium for a line load normal to the surface and one inclined 30 degrees.

2.1 Measuring Strain

Since our plane strain assumption gives a change in volume that depends only on the strain in the x direction, there are some implications for volume dependent strain sensors. Figure 4 shows how a transducer based on the volume resistance could be used to determine the strain at a certain depth. Consider a block of conductive material with the electrodes on the top and bottom. The resistance is given by:

$$R = \frac{\rho L}{A} = \frac{\rho x}{yz} \tag{9}$$

where ρ is the resistivity, R is the resistance, L is the length, and A is the area.

For plane strain the new dimensions are:

$$x' = x(1+\varepsilon_x)$$

$$y' = y(1+\varepsilon_y) = y(1-\varepsilon_x) \text{ since } \varepsilon_y = -\varepsilon_x$$

$$z' = z$$

For a unit volume element

$$R = \frac{\rho(1+\varepsilon_x)}{(1-\varepsilon_x)} \approx \rho(1+\varepsilon_x)(1+\varepsilon_x+\varepsilon_x^2+\cdots) \approx \rho(1+2\varepsilon_x) \tag{10}$$

This transducer would output the variable of interest. A similar result can be shown for the plane

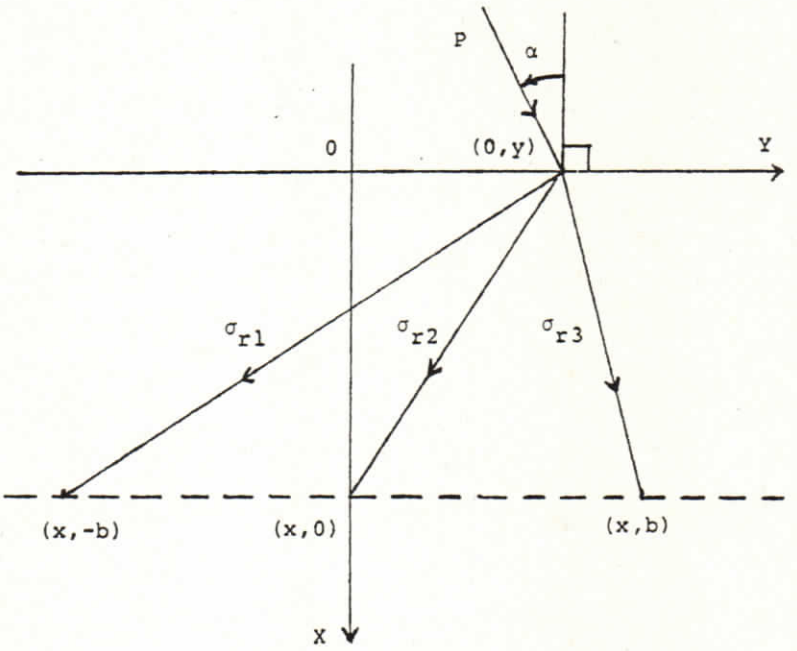

Figure 5. Three Equally Spaced Strain Sensors

stress assumption:

$$R = \frac{\rho(1+\varepsilon_x)}{(1+\varepsilon_y)(1+\varepsilon_z)} \approx \rho(1+\varepsilon_x-\varepsilon_y-\varepsilon_z) = \rho(1+2\varepsilon_x)$$

$$\text{since} \quad -\varepsilon_z = \varepsilon_x+\varepsilon_y \tag{11}$$

3.0 Determine Force Angle for a Line Load

Can the angle of inclination, location, and magnitude of a line load be recovered from the type of sensor described previously, that measures only one parameter, ε_x? Assuming negligible sensor dimensions, it is straight forward to set up the equations for three strain sensors equally spaced on a horizontal plane beneath the surface. Referring to Figure 5 they are:

$$\varepsilon_{x_1} = \frac{-3P\left[x\cos\alpha - (y+b)\sin\alpha\right]}{2\pi E\left[x^2+(y+b)^2\right]^2}\left[x^2 - (y+b)^2\right]$$

$$\varepsilon_{x_2} = \frac{-3P\left[x\cos\alpha - y\sin\alpha\right]}{2\pi E(x^2+y^2)^2}\left[x^2 - y^2\right] \tag{12}$$

$$\varepsilon_{x_3} = \frac{-3P\left[x\cos\alpha - (y-b)\sin\alpha\right]}{2\pi E\left[x^2 + (y-b)^2\right]^2}\left[x^2 - (y-b)^2\right]$$

where x is the sensor depth and b is the sensor spacing.

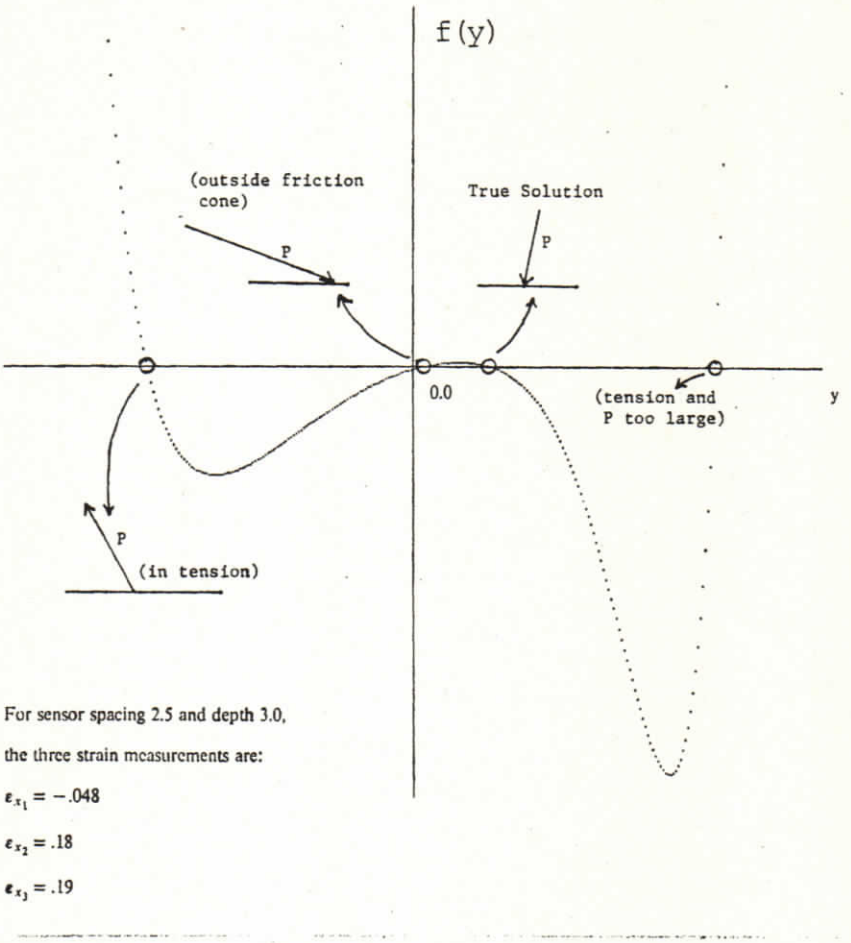

Figure 6. Finding the Force Location with Multiple Roots

We can use "equation counting" methods [Richards, Rubin, and Hoffman, 1981] to determine if these 3 measurements are sufficient to uniquely determine the line load on the surface. The implicit function theorem [Sokolnikoff and Redheffer 1966] states that if the system of equations (12) is continuous and has continuous first partial derivatives with respect to the independent variables, and if the Jacobian is non-zero, then there will be a unique and continuous solution to those equations. The determinant of the Jacobian of eq. (12) is not identically zero, but does disappear for some values of parameters.

To determine where the extra solution points are, the system of equations was solved by elimination of the magnitude and angle of the force, to get a polynomial in y and the measured strains:

$$f(y) = 2\epsilon_{x_2}\left[x^2 + y^2\right]^2\left[x^2 - (y-b)^2\right]\left[x^2-(y+b)^2\right]$$

$$- \epsilon_{x_1}\left[x^2 + (y+b)^2\right]^2\left[x^2 - y^2\right]\left[x^2 - (y-b)^2\right] \qquad (13)$$

$$- \epsilon_{x_3}\left[x^2 + (y-b)^2\right]^2\left[x^2-y^2\right]\left[x^2 - (y+b)^2\right] = 0$$

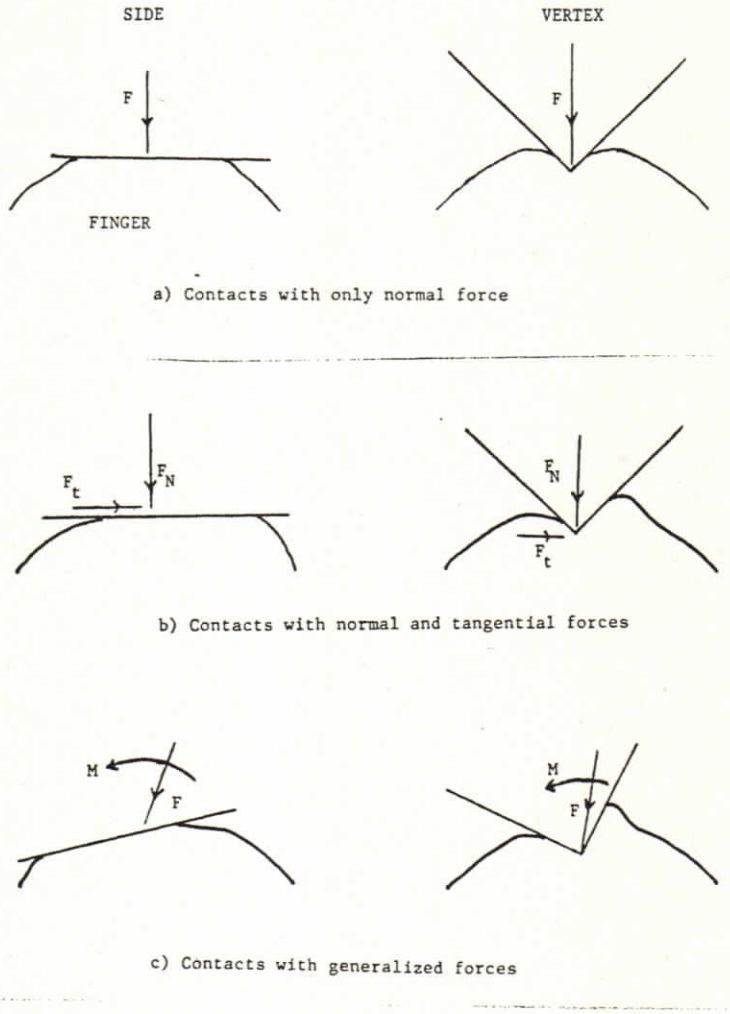

Figure 7. Finger Contacts with Side and Vertex

This eighth degree polynomial has multiple real roots close to the sensor locations. It is interesting to note that if the sensor depth and the spacing are equal ($x=b$), one of the false roots will always be at $y=0$. Constraints on the possible forces, such as magnitude ranges and angle limits, allow some of these solutions to be rejected. For example, a reasonable constraint is that all forces are directed into the surface (compressive). Tension will not occur at the contact without an adhesive bond. If there are still possible roots left, a fourth sensor measurement will be necessary to get a unique solution.

Figure 6 shows an example with false roots that can be discarded. Two can be rejected because the point force would have to be in tension, and one other because the force is too close to horizontal and would slip.

4.0 Distinguish a Vertex from a Side

In this section, we will try to differentiate between the strains beneath the skin due to the vertex and the side contacts. Figure 7 shows the assumptions used for these contacts. Assume the side is perpendicular to the finger and is moving perpendicularly into the skin. For the vertex, assume its center line is perpendicular to the edge of the finger and is moving perpendicularly into the skin. These can be viewed as contacts with a normal force but no moment (Figure 7a).

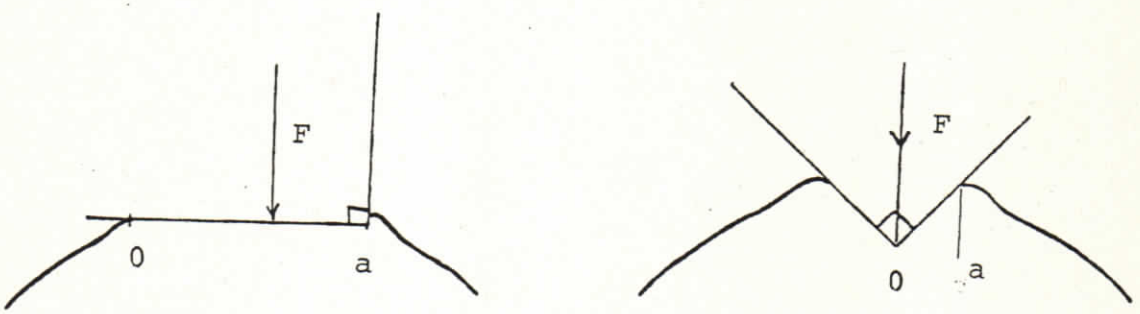

Figure 8. Two Extreme Vertex Cases

Figure 7b shows normal contacts with a tangential force. The most general case of a moment and a traction force is shown in Figure 7c. Restricting the analysis to the 2 dimensional case with plane strain, we will attempt to characterize the strains that would be measured for normal contacts without a tangential force.

For this analysis, we will ignore traction from friction while indenting normally into the elastic medium. With friction present, the elastic medium would adhere to the object and cause surface shear stresses as it tried to flow away from the indentation. The normal stresses are not affected very much by this traction effect [Engel and Conway, 1971].

What does a vertex feel like? Consider the vertexes touching the finger as in Figure 8. The first case appears to be the right side of a rectangular indenter. If we could consider the finger and the contacting side extending far away from the right side, then the left side of the indenter would have no effect on the right side. The surface stress for a rectangular indenter on an elastic half plane is given by [Conway, Vogel, Farnham and So, 1966]:

$$\sigma_x(x = 0) = \begin{cases} \dfrac{P}{\pi\sqrt{a^2-y^2}} & \text{for } |y| < a \\ 0 & \text{otherwise} \end{cases} \tag{14}$$

where P is the force per unit length, and a is the half width of the contact.

The second case is equivalent to a wedge of 90 degrees being pressed into an elastic half plane. This stress is given by [Gladwell 1980; Robinson and Thompson 1974] as:

$$\sigma_x(x = 0) = \begin{cases} K\cot\dfrac{\theta}{2}\cosh^{-1}\dfrac{a}{|y|} & \text{for } |y| < a \\ 0 & \text{otherwise} \end{cases} \tag{15}$$

where K is a function of Poisson's ratio and the modulus of elasticity, and θ is the vertex angle.

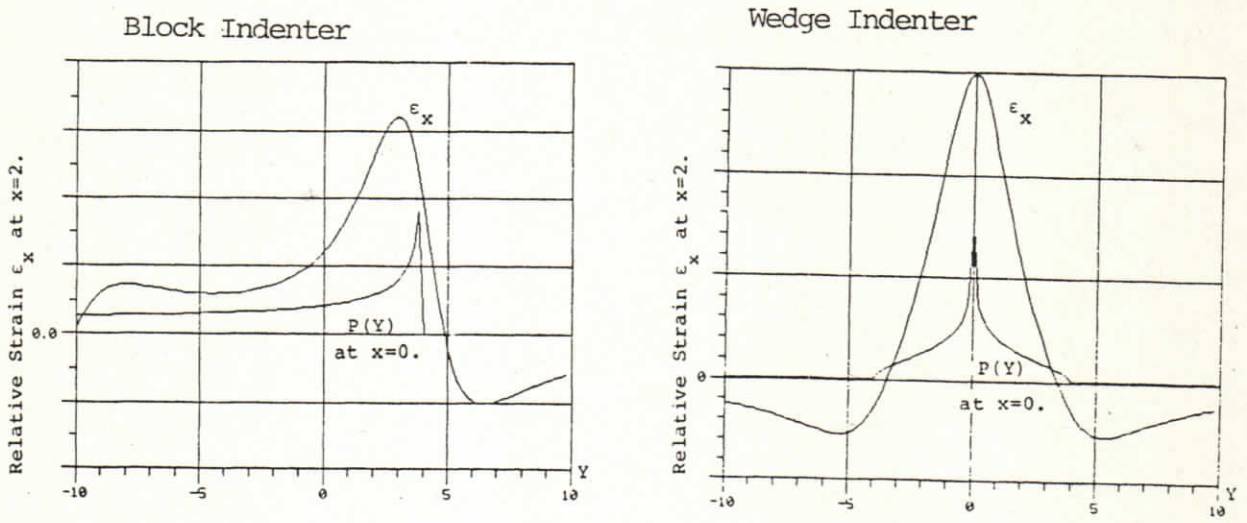

Figure 9. Stresses and Strains for Vertexes

Figure 9 shows the stresses and strains for these vertex contacts. A vertex looks very much like a line load especially for small indentations and small vertex angles. If the line load and vertex have approximately the same strain profiles, the method of section 3.0 could be used to find the angle of force at this contact.

Now consider the contact of a stiff flat side and a circular elastic finger as in Figure 10a. This two dimensional problem is difficult to analyze analytically, so we will apply Saint-Venant's Principle, as explained by Timoshenko [1951]:

This principle states that if the forces acting on a small portion of the surface of an elastic body are replaced by another statically equivalent system of forces acting on the same portion of the surface, this redistribution of loading produces substantial changes in the stresses locally but has a negligible effect on the stresses at distances which are large in comparison with the linear dimensions of the surface on which the forces are changed.

If the area of contact is small compared to the finger radius, we can approximate the area near the contact as an infinite elastic half plane. This approximation will be most accurate near the outer surface of the finger in the quadrant where the contact is. It is also necessary to reformulate the contact stresses for the cylindrical finger to match the half plane approximation.

In the solid mechanics literature, the common problem is the rigid cylinder indenting an elastic layer, the punch problem, rather than an elastic cylinder contacting a rigid plane. Bentall and Johnson [1968] have done an analysis where the elasticity of the cylinder and layer are equal. Hahn and Levinson [1974] have analyzed the stresses for the contact of a rigid cylinder and a cylinder covered with an elastic layer. That analysis is probably most relevant to the rigid finger with an elastic covering contacting a rigid surface, but as in much of the contact literature, the form of the solutions (infinite series) is inconvenient to work with.

For a rigid cylinder indenting an elastic half plane, as in Figure 10b, the stress on the surface is given by Conway [1966] as:

$$\sigma_x(y) = \frac{2P}{\pi a^2}\sqrt{a^2 - y^2} \tag{16}$$

where a is the half width of the contact region and P is the force per unit length on the cylinder. The stress and strain for this contact are shown in Figure 11.

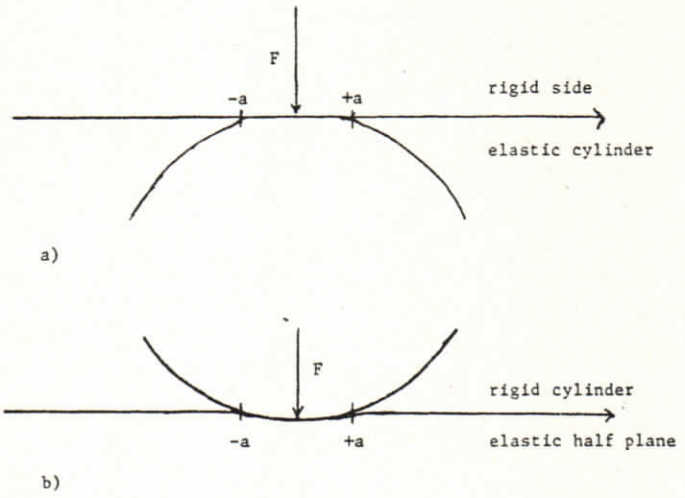

Figure 10. Approximating a Contact with a Side

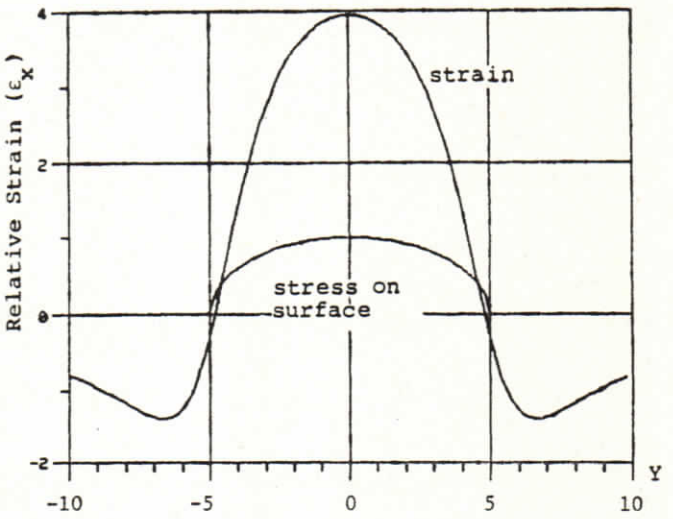

Figure 11. Stresses and Strains for Cylindrical Indentor

The half width of the contact from [Bentall and Johnson, 1968] is:

$$a = 2\left[\frac{4RP(1-\nu^2)}{\pi E}\right]^{\frac{1}{2}} \tag{17}$$

where R is the radius of the cylinder.

For equilibrium in the contact region, the stresses should be equal and of opposite sign on the cylinder and the surface. Now for an elastic cylindrical finger contacting a side, there should be no infinite stresses such as occur at sharp edges of indentations. Also, the stress will have a peak value in the center of the contact, and approach zero at the edges. Using this justification, we will assume that the stress on the finger can be approximated by eq. (16) for small indentations.

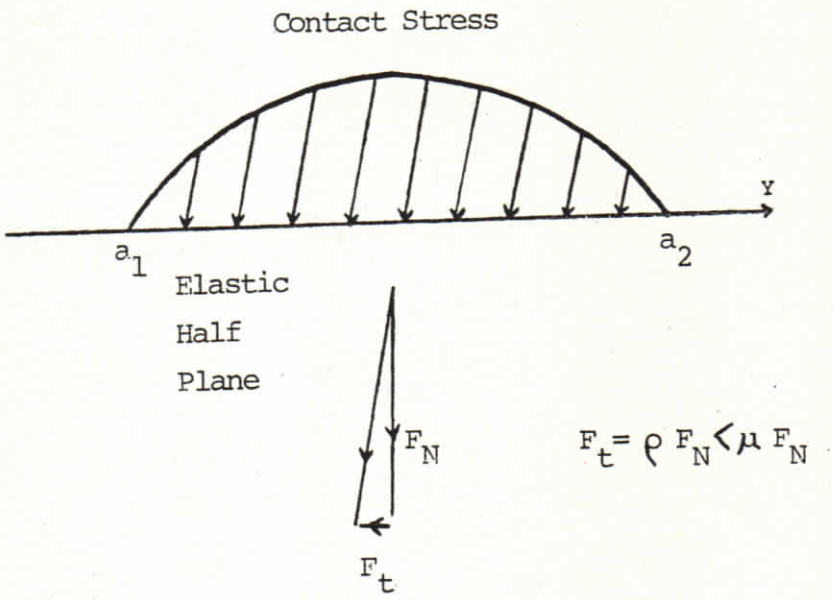

Figure 12. Tangential Stress Proportional to Normal Stress

The stresses due to contacting a side and a vertex are distinguishably different. For the side, there is a smooth, continuous stress function. For the vertex, there is a discontinuity in the stress at the tip of the wedge. (Actually, the medium deforms around that discontinuity, spreading the stress over a finite area). It should be easy to distinguish the two just by looking at the width of the strain pattern. For the same elasticity and pressure, the wedge has greater indentation depth with a smaller contact area than the side contact. If the vertex angle is less than 90 degrees, there will be a significant difference between the two contact widths. Arguably, this task would be simpler if the indentation profile were available.

5.0 Determining the Side-Finger Contact Force

For a finger touching the side, we will assume that the contact is of the form shown in Figure 7b, with both normal and tangential components, but no moment. The tangential components will be modeled as all being in the same direction with a force that is directly proportional to the magnitude of the normal force [Smith and Liu, 1953]. Figure 12 shows this assumption for a general pressure pattern. (The tangential force must be less than μN, the friction force).

A very complicated expression for the stress below the surface for an elliptical stress distribution on the boundary was found by Smith and Liu [1953]. We do not need the complete stress expression, but want to determine the angle of force at the contact. For grasping applications, the angle of force α is useful for predicting slip.

To find the strain underneath for the stress for the cylindrical indentor from eq. (16), we integrate along the surface where

$$P(y) = \begin{cases} \frac{2P}{\pi a^2}\left[a^2 - \left(y - \frac{a_1+a_2}{2}\right)^2\right]^{\frac{1}{2}} & \text{for } a_1 < y < a_2 \\ 0 \text{ otherwise} \end{cases} \tag{18}$$

where a_1 and a_2 are the edges of the contact, and $a = a_2 - a_1$. Applying the superposition

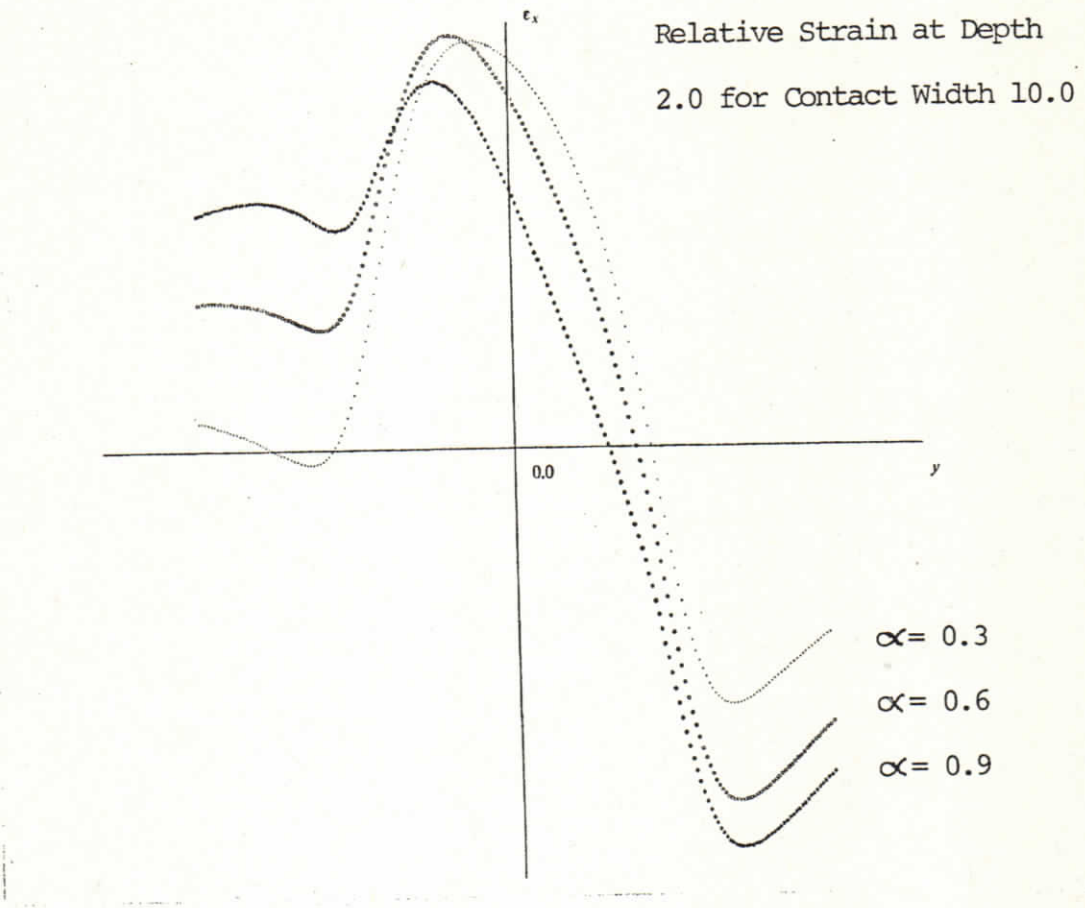

Figure 13. Strain for Cylinder Contact with Tangential Loads

principle to the strain due to a line contact eq. (8):

$$\epsilon_x(x,y) = \int_{-\infty}^{\infty} \frac{-3\left[x\cos\alpha - y_o\sin\alpha\right]\left[x^2-{y_o}^2\right]P(y-y_o)}{2\pi E r^4}\,dy_o \tag{19}$$

Substituting the integration limits for $P(y)$ gives:

$$\epsilon_x(x,y) = \frac{-3P}{\pi^2 a^2 E}\int_{y-a_2}^{y-a_1}\left[\frac{x\cos\alpha - y_o\sin\alpha}{(x^2+{y_o}^2)^2}\right]\left[x^2-{y_o}^2\right]\left[a^2-(y-y_o-\frac{a_1+a_2}{2})^2\right]^{\frac{1}{2}}dy_o \tag{20}$$

where $r^2 = x^2+{y_o}^2$.

Figure 13 shows the strain for the cylindrical indentor with various tangential loads applied. Note that the slope of the strain underneath the center of the contact increases with increasing tangential force. The slope of $\epsilon_x(x,y)$ at $y = (a_1+a_2)/2$ can be found by evaluating the derivative of eq. (20), using the first fundamental theorem of integral calculus to get:

$$\frac{d\epsilon_x}{dy} = -\frac{3\sqrt{3}P}{2\pi^2 aE}\left[x^2-(\frac{a}{2})^2\right]\left[x^2+(\frac{a}{2})^2\right]^{-2}\sin\alpha \tag{21}$$

When the contact length is large compared to the sensor depth, this simplifies to

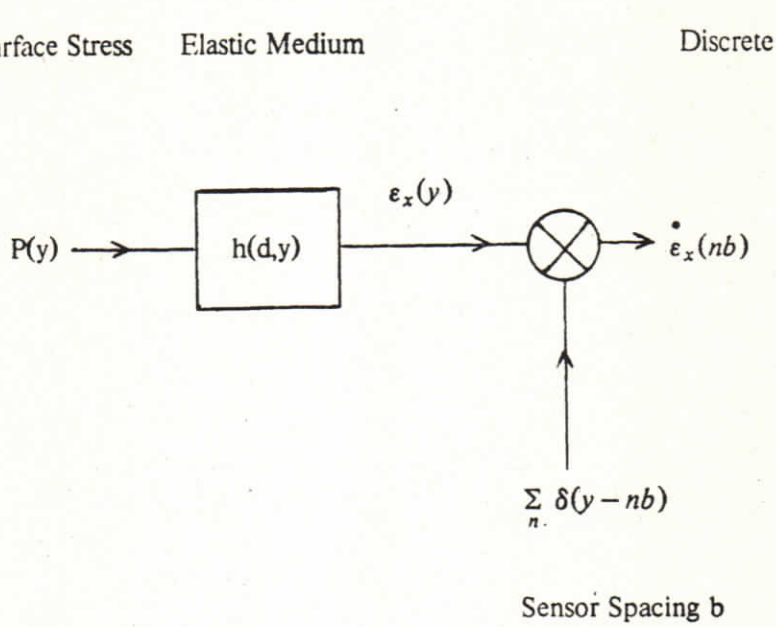

Figure 14. Discrete Strain Measurements

$$\frac{d\varepsilon_x}{dy} \approx \frac{-6\sqrt{3}P\sin\alpha}{\pi^2 a^3 E} \tag{22}$$

So for a given contact, α can be easily recovered if the pressure can be estimated.

The more complicated contact with generalized forces of Figure 7c can be treated as the superposition of stresses due to forces plus the stresses due to the moment load. The elasticity literature deals with moments applied to punches indenting an elastic medium [Alblas and Kuipers, 1970; Galin 1961]. In those cases, the pressure distribution due to the moment load is an odd function symmetric about the origin, with half the surface in tension and the other half in compression, so the moment can significantly affect the internal strains.

6.0 Sensor Density Requirements

In section 3, a method to determine the location, direction, and magnitude of a line contact was outlined that required at least three strain sensors. A more general question is, how many strain sensors are needed to identify a general stress pattern on the surface? This problem is considered in the context of the spatial frequencies of the applied stress. The spatial frequency of the stress pattern is just the variations in pressure per unit length, not time dependent variations. We shall assume that the pressure pattern is approximately bandlimited, that is, most of the stress spectrum is concentrated at low frequencies. This is the case for contact stresses in the form of (15) and (16).

Figure 14 shows a linear system representation of this discrete measurement process, where the sensors are of negligible width. The sampling theorem says that any bandlimited signal can be recovered from its discrete samples if the samples are taken at a sufficiently high frequency, the Nyquist rate. (For example see [Oppenheim and Schafer, 1975]). Here the sampling frequency is the minimum strain sensor spacing needed to avoid aliasing when recovering the continuous strain measurements from the discrete samples. If there are not enough sensors, the strain due to the high frequency components will appear as noise when the continuous strain is recovered from the samples by low pass filtering.

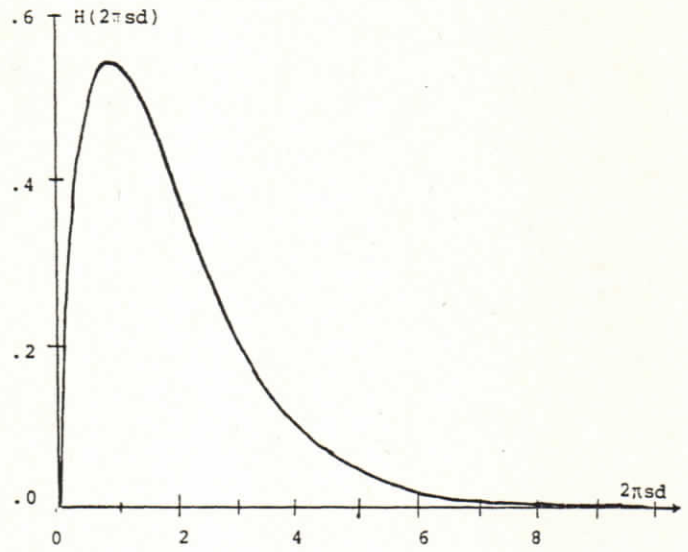

Figure 15. Spatial Frequency Response of Elastic Medium

Since the strain at a point beneath the surface is a linear function of the two stress components σ_x and σ_y for plane strain, the total strain at a point in the elastic medium can be found by the superposition of the strains underneath due to each stress component on the surface. It should be possible to treat the normal and tangential stresses separately, and determine the highest frequencies of interest for each. If the force on the boundary has no tangential components, the pressure distribution $P(y)$ will be a scalar at each point. The superposition integral is:

$$\varepsilon_x(d,y_o) = \int_{-\infty}^{\infty} \frac{P(y)}{E} h(y_o - y)\, dy \tag{23}$$

where $P(y)$ is the pressure distribution on the surface and $h(y)$ is the strain at depth d due to a unit normal pressure point at the origin. From equation (8):

$$h(y) = \frac{-3\,d(d^2-y^2)}{2\pi\,(d^2+y^2)^2} \tag{24}$$

The spectrum of the "impulse response" $h(y)$ can be found from simple properties of Fourier transforms:

$$\frac{d}{\pi(d^2+y^2)} \longleftrightarrow e^{-d|2\pi s|}$$

$$\frac{d^2}{\pi(d^2+y^2)^2} \longleftrightarrow \pi e^{-d2\pi s}\left[\frac{1}{d2\pi} + s\right] \text{ for } s > 0$$

$$\frac{dy^2}{\pi(d^2+y^2)^2} \longleftrightarrow \pi d e^{-d2\pi s}\left[\frac{1}{d2\pi} - s\right] \text{ for } s > 0$$

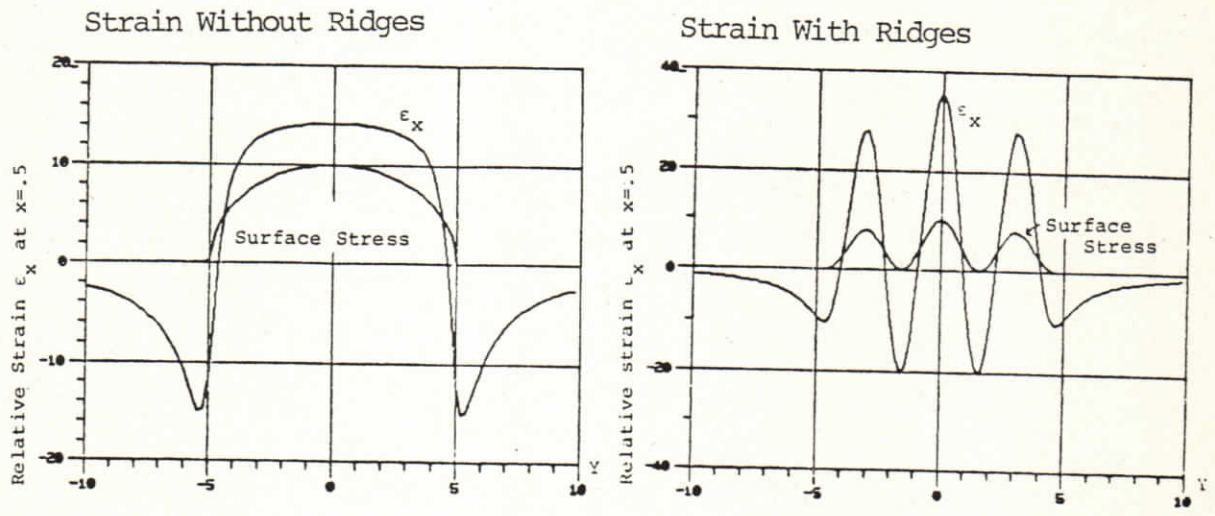

Figure 16. Effect of Ridges on Strain Amplitude

$$\frac{-3d(d^2-y^2)}{2\pi(d^2+y^2)^2} \longleftrightarrow -3\pi ds e^{-d|2\pi s|} = H(s) \tag{25}$$

The incompressible medium in plane strain has no response to a zero spatial frequency, that is, a constant pressure over an infinite extent, because there is no space for the medium to escape into.

The frequency response of the elastic medium as shown in Figure 15 is not strictly bandlimited, but it does have very steep skirts. We shall assume that the overall frequency response $P(s)H(s)$ has a high frequency response like $H(s)$, where $P(s)$ is the pressure spectrum.

We can choose a sampling frequency by deciding how much aliasing is permissible. This requires an engineering judgement based on the estimated accuracy of the strain sensors. It seems that any aliasing that was less than one part in 1000 of full scale would be negligible because most sensors would not have a dynamic range much better than that. Also, non-linearities and temperature instabilities get to be of at least the same order of magnitude.

The following rough estimate can be used for sampling requirements. We want the value at the tail to be down a factor of 1000 from the maximum which occurs at $2\pi sd = 1$. So:

$$\frac{e^{-1}}{fe^{-f}} = 10^3 \text{, or } f = 10.2 \tag{26}$$

The samples should be at twice f so $2\pi sd \geq 20.4$, or $sd > 3.2$. Here s is the number of samples per unit length.

For a sensor depth of 1.0, a sensor density of 3.2 sensors per unit distance would allow recovery of the continuous strain response due to a normally directed surface stress distribution with aliasing errors down at least a factor of 1000 from the desired signal. This sampling rate is probably too conservative. The types of features touched may have rounded edges, and start out with a more band limited signal, so a lower sensor density could be adequate. The effective sensor density can be increased by multiple measurements as a finger is moved along a surface, so the ultimate frequency response is limited by the number of samples per second, and the sensor accuracy.

6.1 Using Finger Ridges to Enhance Sensitivity

The infinite elastic medium has a peak response when the wavelength equals the strain sensor depth times 2π. There seems to be an interesting possibility of maximizing the strain sensors' outputs by locating them at the maxima and minima of strain, and predetermining the frequency and phase of the pressure. This could be done in principle by inserting a thin and flexible sinusoidal grating between the finger and the object touched, which could superimpose a sinusoidal stress on the regular stress. A simple method of adding the sinusoid of the desired frequency is to use a ridged finger.

In Figure 16 we compare the strain amplitude between the unridged and ridged fingers, where the ridges are of the optimal wavelength. In both cases the sensors are at the same depth. In the unridged case the total contact stress is about 1.5 times the ridged case. Even neglecting the difference in total contact stress, the ridges can enhance the amplitude by a factor of 2. The sensors should be located beneath and between ridges to detect the maximum amplitude peaks. This technique is similar to the electrical chopper that allows a DC level to pass through an AC coupled circuit.

It is curious to note that in the human finger, there is a mechanoreceptor located directly beneath every papillary ridge [Lederman, 1978]. Phillips and Johnson [1981] gave the depth of this strain measuring mechanoreceptor in the macaque monkey as about 500 μm. This is about the same depth as in the human finger [Quilliam 1978]. The optimum ridge spacing for this depth is about 3 mm, much larger than the papillary ridge spacing on the authors' fingers. However, it is interesting to speculate that fingerprints may still have some role in enhancing strain measurements.

7.0 Discussion

What effect does the skin compliance have on tactile sensing abilities? A stiffer skin will develop greater contact stresses for the same indentation, but the subsurface deformations (the measured strain) will be the same [Phillips and Johnson, 1981]. The smaller contact area and deformation with a less compliant material helps to make the approximations we have used more valid. Greater stiffness in the skin may also serve to protect the sensors because a stiffer skin has more resistance to puncture.

A very compliant skin on a sensor may have saturation effects sooner than a harder skin. Figure 17 shows three fingers applied to a surface with the same normal force, but with different covering softness. For the very stiff skin, the contact is not large enough to determine the size of the particle. For the very soft skin, the stress due to the small particle may become proportionally less significant than the stress due to contact with the surface around the particle. One way to choose a skin compliance for good sensing characteristics would be to decide on a typical finger force range and the smallest contact area of interest, and use this information to determine the necessary modulus of elasticity.

An area for further research is the spatial bandwidth that is required for feature recognition. The two-point discrimination test [Valbo and Johanson 1978], seems to be the classic test for tactile sensor resolution. This test would seem to require a very high bandwidth because of the two impulse functions, but it may turn out that only the low frequencies are important. While we are

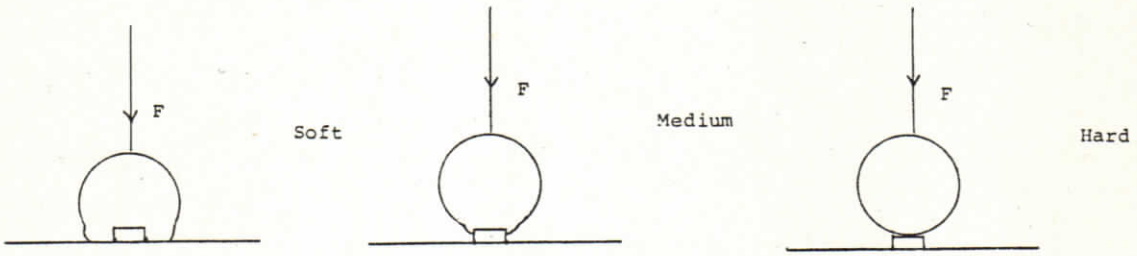

Figure 17. Contacts for Different Skin Compliances

not interested in resolving between two point indenters, this problem may be useful for setting a smaller upper bound on the density of sensors.

In psychophysical experiments, subjects are instructed that there will either be one or two points indenting their skin. It appears that the sensors should be able to distinguish between these two cases for two-point distances significantly smaller than the individual receptive fields of each sensor. Here, the resolution is not limited by the density of the sensors, but by the measurement accuracy of the sensors.

It is useful to consider each strain sensor as having a response function that overlaps its neighbor. A point force on the surface will cause an output for each sensor that is proportional to the height of the response function underneath that point. For two point forces on the surface, the outputs will be the linear superposition of the responses of each point force. We can measure the output in each sensor channel, and determine if it is consistent with just a single point force. However, there might be different combinations of point forces that can give the same output. A very loose analogy can be made to the color matching problem [Richards, 1979], where several different stimulation combinations can give a white sensation.

In Figure 18 there are locations where two point forces can be applied that will give a response in the two sensors equivalent to a single point force. In Figure 19, a third sensor has been added to allow discrimination between all the two point and one point cases, limited by the measurement accuracy. It will be difficult to distinguish points that give responses far down on the "tails" of the channel.

It is probably reasonable not to spread the sensors too far apart. A guess is that the practical maximum separation would be less than twice the depth of the sensors. (Note that for the two-point discrimination task, the modulus of elasticity has no effect on the width of the strain response, so it will have no effect on the resolution). More work should be done on choosing the depth and sensor spacing to optimize discrimination.

It seems that some recognition tasks would be easier using a sensor that responded to deformation. That would make distinguishing a vertex and a side easy work. However, other tasks, such as sensing imminent slip, appear easier with the strain sensor approach. Sensors that combine surface shear sensors, depth strain sensors, and surface deflection sensing would simplify the problem considerably.

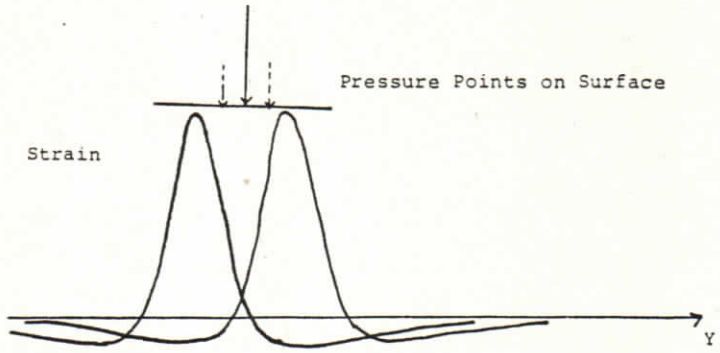

Figure 18. Two Strain Response Sensors

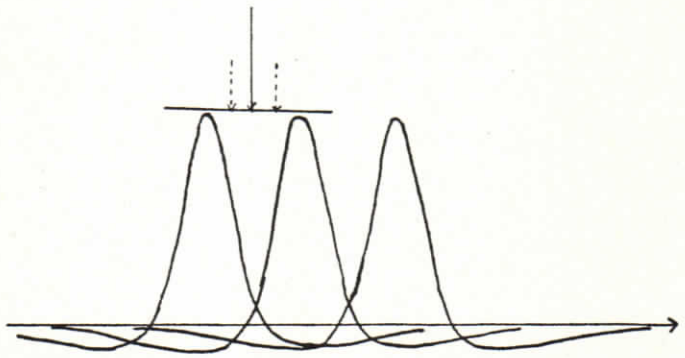

Figure 19. Three Strain Response Sensors

8.0 Conclusion

In this paper, we used a simple linear elastic model to predict strains beneath a compliant skin for a finger touching a knife edge (line load), a corner, and a flat surface. Appropriate approximations were made to get simple expressions for the contact stresses for a cylindrical finger contacting a side. In general, three strain measurements were shown to be necessary for determining the location, magnitude, and direction of force for a line contact, but degenerate cases with multiple solutions are possible. The angle of force was shown to be related to the slope of the strain curve for a contact with a side. Further work needs to be done in recovering the angle of force from contacts with other curvatures.

The elastic medium was examined as a signal processing element, which led to the interesting possibility of maximizing strain sensor output by adding a grating to the sensor surface with a period equal to the sensor depth times 2π.

We have not attempted to determine stresses and strains for the generalized three dimensional contact. At least five strain measurements are required to determine the magnitude, two angles, and y,z location of a point force on an elastic half-space. These equations are quite complicated [Mindlin, 1936]. It may be possible to find this information by combining two orthogonal planar solutions, but this was not attempted here.

The discussion here seems to indicate that four sensors, with fairly high dynamic range, may be adequate for the planar case for finding force magnitudes and directions, and for distinguishing between two contact types (vertex and side). With a thick skin, one can get a lot from a few sensors. This number of sensors will probably not suffice for determining curvature and more complicated force resolving problems.

References

[1] J.B. Alblas and M. Kuipers, "Contact problems of a rectangular block on an elastic layer of finite thickness, part II: The thick layer," *Acta Mechanica* Vol. 9, pp. 1-12, 1970.

[2] R.H. Bentall and K.L. Johnson, "An elastic strip in plane rolling contact," *Int. J. Mech. Sci.* Vol. 10, pp. 637-663, 1968.

[3] H.D. Conway, S.M. Vogel, A. Farnham, and S. So, "Normal and shearing contact stresses in indented strips and slabs," *Int. J. Engineering Sci.* Vol. 4, pp. 343-359, 1966.

[4] P.A. Engel and H.D. Conway, "Contact stress analysis for an elastic cylinder indenting a slab in the presence of friction," *Int. J. Mech. Sci.* Vol. 13, pp. 391-402, 1971.

[5] R.S. Fearing, "Simplified grasping and manipulation with dextrous robot hands", American Control Conference, San Diego, CA June, 1984.

[6] R.S. Fearing, "Touch processing for determining a stable grasp", S.M. Thesis, MIT EE&CS, Sept. 1983.

[7] L. Galin, *Contact Problems in the Theory of Elasticity,* [I.N. Sneddon, Editor] N. Carolina State College, Raleigh N.C. 1961.

[8] P.C. Gaston and T. Lozano-Perez, "Tactile recognition and localization using object models: the case of polyhedra on a plane," M.I.T. A.I. Memo, March, 1983.

[9] G.M.L. Gladwell, *Contact Problems in the Classical Theory of Elasticity,* Alphen an den Rijn, Netherlands: Sijthoff and Noordhoff, 1980.

[10] H.T. Hahn and M. Levinson, "Indentation of an elastic layer bonded to a rigid cylinder-I. Quasistatic case without friction," *Int. J. Mech. Sci.* Vol. 16, pp. 480-502, 1974.

[11] W.D. Hillis, "Active Touch Sensing," S.M. Thesis, MIT EE&CS, Jan. 1981.

[12] G.I. Kinoshita, "Classification of grasped object's shape by an artificial hand with multi-element tactile sensors," *IFAC Symposium on Information Control Problems in Manufacturing Technology,* Tokyo 1977, pp. 111-118.

[13] S.J. Lederman, "Heightening tactile impressions of surface texture," in *Active Touch,* edited by G. Gordon, pp. 205-214, Pergamon Press, 1978.

[14] R. Masuda, K. Hasegawa, and K. Osako, "Slip sensor of industrial robot and its application," *Electrical Engineering in Japan,* Vol. 96, No. 5, 1976.

[15] R.D. Mindlin, "Force at a point in the interior of a semi-infinite solid," *Physics*, Vol. 7, pp. 195-202, May, 1936.

[16] A.V. Oppenheim and R.W. Schafer, *Digital Signal Processing*, Prentice-Hall, 1975.

[17] K.J. Overton and T. Williams, "Tactile sensation for robots," *IJCAI-81*, pp. 791-795, 1981.

[18] H. Ozaki, S. Waku, A. Mohri, "Pattern recognition of a grasped object by unit-vector distribution," *IEEE Transactions on Systems, Man, and Cybernetics* SMC-12, No. 3, May/June 1982.

[19] C.J. Page, A. Pugh, and W.B. Heginbotham, "New techniques for tactile imaging," *Radio and Electronic Engineer*, Vol. 46, No. 11, pp. 519-526, November 1976.

[20] J.R. Phillips and K.O. Johnson, "Tactile spatial resolution III. A continuum mechanics model of skin predicting mechanoreceptor responses to bars, edges, and gratings," *J. of Neurophysiology* 46: 1204-1225, 1981.

[21] T.A. Quilliam, "The structure of fingerprint skin," in *Active Touch*, edited by G. Gordon, pp. 1-15, Pergamon Press, 1978.

[22] W.A. Richards, "Quantifying sensory channels: generalizing colorimetry to orientation and texture, touch, and tones," *Sensory Processes 3*, pp. 207-229, 1979.

[23] W.A. Richards, J.M. Rubin, and D.D. Hoffman, "Equation counting and the interpretation of sensory data," MIT AI Memo No. 614, June 1981.

[24] A.R. Robinson and J.C. Thompson, "Transient stresses in an elastic half space resulting from the frictionless indentation of a rigid wedge shaped die," *Zeitschrift fur Angewandte Mathematik und Mechanik*, vol. 54, pp.139-144, 1974.

[25] J.O. Smith and C.K. Liu, "Stresses due to tangential and normal loads on an elastic solid with application to some contact stress problems," *J. of Appl. Mechanics, Trans. ASME*, Vol. 75, pp 157-166, 1953.

[26] I.S. Sokolnikoff and R.M. Redheffer, "Mathematics of Physics and Modern Engineering," McGraw-Hill, 1966.

[27] Z. Stojiljkovic, and J. Clot, "Integrated behavior of artificial skin," *IEEE Transactions on Biomedical Engineering*, Vol. BME-24, No. 4, July 1977.

[28] S. Timoshenko and J.N. Goodier, *Theory of Elasticity*, New York: McGraw-Hill 1951.

[29] A.B. Valbo and R.S. Johanson, "The tactile sensory innervation of the glabrous skin of the human hand," in *Active Touch*, pp. 29-53, edited by G. Gordon, Pergamon Press, 1978.